Cryogenics 49 (2009) 226–234

Contents lists available at ScienceDirect

Cryogenics

journal homepage: www.elsevier.com/locate/cryogenics

Thermodynamic design of methane liquefaction system based on reversed-Brayton cycle

Ho-Myung Chang [a,*], Myung Jin Chung [a], Min Jee Kim [a], Seong Bum Park [b]

[a] Mechanical Engineering, Hong Ik University, 72-1 Sangsu-Dong, Mapo-Gu, Seoul 121-791, Republic of Korea
[b] Hansol EME Co. Ltd., Gyeonggi-Do 463-824, Republic of Korea

ARTICLE INFO

Article history:
Received 13 March 2008
Received in revised form 7 August 2008
Accepted 27 August 2008

Keywords:
B. LNG
B. Methane
C. Thermodynamics
E. Brayton cycle
E. Heat exchangers

ABSTRACT

A thermodynamic design is performed for reversed-Brayton refrigeration cycle to liquefy methane separated from landfill gas (LFG) in distributed scale. Objective of the design is to find the most efficient operating conditions for a skid-mount type of liquefaction system that is capable of LNG production at 160 l/h. Special attention is paid on liquefying counterflow heat exchanger, because the temperature difference between cold refrigerant and methane is smallest at the middle of heat exchanger, which seriously limits the overall thermodynamic performance of the liquefaction system. Nitrogen is selected as refrigerant, as it is superior to helium in thermodynamic efficiency. In order to consider specifically the size effect of heat exchangers, the performance of plate-fin heat exchangers is estimated with rigorous numerical calculations by incorporating a commercial code for properties of methane and the refrigerant. Optimal conditions in operating pressure and heat exchanger size are presented and discussed for prototype construction under a governmental project in Korea.

1. Introduction

One of the main governmental efforts to utilize renewable energy and reduce greenhouse gas in Korea is the development of domestic liquefaction technology of methane separated from landfill gas (LFG). Methane is a major component (45–55% by volume) of typical LFG mixture at domestic waste landfill sites, and can be stored and transported conveniently as liquefied natural gas (LNG) with high energy density at a moderate pressure. The LFG-to-LNG conversion is involved of several different technical issues [1,2], one of which is efficient cryogenic refrigeration to continuously liquefy methane in a distributed scale. According to Barclay et al. [3], the term "distributed scale" refers to liquefiers with LNG production capacities of 160–2350 l/h (or 1000–15,000 gallons per day).

In 2007, the Korea New and Renewable Energy Center (KNREC) starts to support a three-year project that will design and develop a prototype for skid-mount type of methane liquefaction system with a capacity of 18.5 g/s (1000 gallons LNG per day). On a successful development of the prototype, it is planned to scale up the system to 92.5 g/s (5000 gallons LNG per day) at the stage of commercial application at SUDOKWON (which verbally means "Metropolitan Seoul") landfill sites. As a first step of the project, thermodynamic design is performed in this study for the purpose of selecting suitable cycle configuration, refrigerant, operating conditions, and heat exchanger size. Since the produced LNG should be competitive (or comparable) in price with imported LNG and the system should be small enough to be packaged onto skids, both thermodynamic efficiency and compactness should be considered in the design process.

In a recent publication, Barclay et al. [3] presented an excellent review on the selection of thermodynamic refrigeration cycle for distributed natural gas liquefaction. Joule–Thomson cycle with MR (mixed refrigerant) is recommended to take advantages of lower capital costs, as it employs a throttle valve (isenthalpic expansion) with two-phase refrigerant. Reversed-Brayton cycle is also recommended to take advantages of simpler design and operating costs, as it employs an expansion machine (nearly isentropic) with gas refrigerant. Another possibility is Claude or Heylandt cycle that combines the isenthalpic and isentropic expansion [4]. Andress and Watkins [5] described their optimized cascade LNG process with highlighting the advantages of safe and easy operation. Some of the commercially available Stirling cryocoolers [6] have refrigeration capacity of 10 kW or greater at liquid nitrogen temperature, which may be directly and conveniently used for these applications.

Reversed-Brayton cycle is selected in this methane liquefaction system, mainly because the two design goals (thermodynamic efficiency and compactness) may be reasonably achieved. Another significant merit of reversed-Brayton cycle in this application is that its thermodynamic performance is less sensitive to the flow rate or concentration of feed gas and more flexible in integrating different purification modules [3]. Standard reversed-Brayton cycle for

* Corresponding author. Tel.: +82 2 320 1675; fax: +82 2 322 7003.
E-mail address: hmchang@hongik.ac.kr (H.-M. Chang).

0011-2275/$ - see front matter © 2008 Elsevier Ltd. All rights reserved.
doi:10.1016/j.cryogenics.2008.08.006

Nomenclature

C	specific heat at constant pressure (J/kg K)
d	hydraulic diameter of rectangular channel (m)
g	gravitational acceleration (m/s^2)
H	heat exchanger height, in Fig. 4 (m)
h	convective heat transfer coefficient (W/m^2 K)
i	specific enthalpy (J/kg)
i_{fg}	latent heat of vaporization (J/kg)
k	thermal conductivity (W/m K)
L	heat exchanger length, in Fig. 4 (m)
l	flow channel height, in Fig. 4 (m)
$\dot{m}$	mass flow rate of refrigerant (kg/s)
$\dot{m}_{LNG}$	mass flow rate of LNG (kg/s)
n	number of plate, in Fig. 4
Nu	Nusselt number
P	pressure (Pa)
P_e	effective perimeter (m)
Pr	Prandtl number
$\dot{Q}$	heat transfer rate (W)
R	gas constant (J/kg K)
r	recuperative ratio, defined by Eq. (16)
Re	Reynolds number
s	specific entropy (J/kg K)
$\dot{S}_{gen}$	entropy generation rate (W/K)
T	temperature (K)
t	plate thickness, in Fig. 4 (m)
U	overall heat transfer coefficient (W/m^2 K)
W	heat exchanger width, in Fig. 4 (m)
w	flow channel width, in Fig. 4 (m)
$\dot{W}$	power for liquefaction (W)
x	quality (mass fraction of vapor in liquid–vapor mixture)
z	coordinate in flow direction (m)

Greek letters

ΔT	temperature difference (K)
γ	specific ratio of gas refrigerant
η	fin efficiency, adiabatic efficiency
μ	viscosity (Pa s)
ρ	density (kg/m^2)

Subscripts

0	ambient
1–7	state of refrigerant
a–d	state of methane
Al	aluminum
c	compressor
e	expander
H, HP	high pressure
L, LP	low pressure
LHX	liquefying heat exchanger
LNG	liquefied natural gas
M	methane
min	minimum
net	net value
opt	optimum
RHX	recuperative heat exchanger
s	saturation

methane liquefaction is schematically shown in Fig. 1a. The cold gas (state 5) discharged from a cryogenic expander absorbs heat from the feed gas (state a) to produce LNG (state d) in a counterflow heat exchanger, called LHX (liquefying heat exchanger). A minor modification is suggested as in Fig. 1b [3], where the feed gas is precooled through the recuperative heat exchanger (RHX) before entering LHX. In this configuration, the low-pressure stream (7–1) absorbs heat simultaneously from the high-pressure stream (3–4) and the feed gas (a–b).

In this paper, it is intended to investigate the fundamentals of thermodynamic design features in the standard and modified Brayton cycles shown in Fig. 1. For simplicity, it is assumed that the feed gas is pure methane, as the separation and purification module for LFG will be independently developed. Special attention is paid to the effect of cycle modification, selection of refrigerant, operating pressure, and size of heat exchangers on the required power required for the liquefaction rate of 18.5 g/s.

2. Selection of refrigerant and cycle configuration

2.1. Thermodynamic efficiency

Liquefaction of gas can be ideally carried out in a system, where every process is reversible or no entropy is generated. By combining energy and entropy balance equations for the ideal system in steady state, the minimum power for the liquefaction is given by

$$\dot{W}_{min} = \dot{m}_{LNG}[(i_{LNG} - i_0) - T_0(s_{LNG} - s_0)] \quad (1)$$

where T_0 is the ambient temperature at which heat is rejected. When methane liquefaction rate is 18.5 g/s and T_0 = 298 K, the minimum power according to Eq. (1) is 19.9 kW. A performance index of liquefaction system is thermodynamic efficiency or FOM (figure of merit), which is defined as the ratio of the minimum to the actual power

$$\text{FOM} = \frac{\dot{W}_{min}}{\dot{W}} \quad (2)$$

The FOM is considered as "second-law" efficiency of a liquefier [7], because the difference between the actual and minimum powers is so-called thermodynamic irreversibility that is equal to the entropy generation rate multiplied by ambient temperature.

$$\dot{W} - \dot{W}_{min} = T_0\dot{S}_{gen} \quad (3)$$

Since the minimum power is dependent only on its properties and the ambient temperature, the entropy generation should be reduced in order to improve thermodynamic efficiency, and the method of entropy generation minimization (EGM) [7] could be a useful tool to maximize thermodynamic efficiency of the liquefaction system.

2.2. Standard reversed-Brayton cycle

This thermodynamic study starts with the simplest case of standard reversed-Brayton cycle shown in Fig. 1a, where methane is liquefied through a counterflow with cold gas at LHX. Since the liquefying process is composed of cool-down (or temperature decreasing) in vapor phase (a–c) and condensation at constant temperature (c–d), there always exists a point denoted by 6 and c where the temperature difference between two streams has a minimum, which complicates the thermodynamic design of the system [4,7].

For simplicity in this and next sections, it is assumed that refrigerant is an ideal gas with a constant specific heat, and methane is also an ideal gas in vapor phase. This assumption is temporary to observe more clearly the fundamental features concerning the selection of refrigerant, and the real properties of refrigerant and methane will be fully considered in following sections. It is further

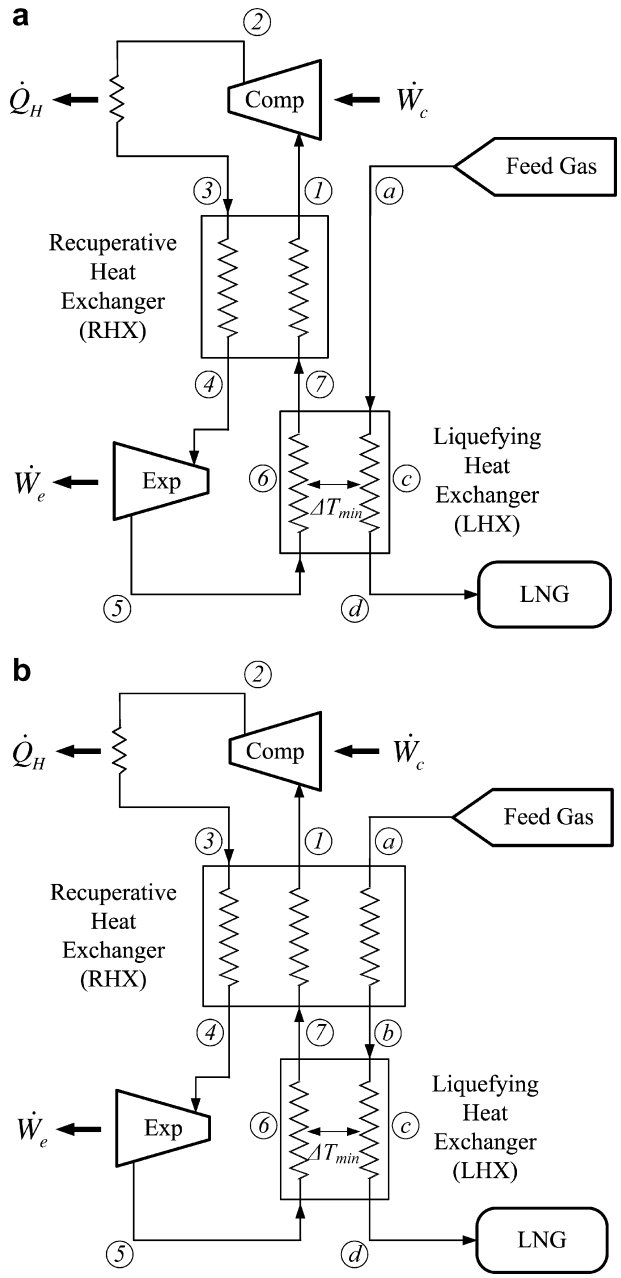

Fig. 1. Methane liquefaction system with reversed-Brayton cycle: (a) standard cycle; (b) modified cycle.

assumed that every heat exchanger is 100% effective with no pressure drop, and the compressor and expander have an adiabatic efficiency of 100%. It is noted again that such a cycle is the limiting case that every single component has its best performance in the given cycle configuration.

As sketched in Fig. 2a, the minimum ΔT in the LHX occurs always at the point of saturate vapor (state c) of methane. It is convenient to consider the LHX as two separate parts such that

$$\dot{m}C(T_7 - T_6) = \dot{m}_{LNG}C_M(T_a - T_c) \quad (4)$$

$$\dot{m}C(T_6 - T_5) = \dot{m}_{LNG}i_{fg} \quad (5)$$

where C and C_M are specific heat at constant pressure of gas refrigerant and methane vapor, respectively, and i_{fg} is latent heat of vaporization of liquid methane. The limiting case of 100% effectiveness is that the temperature difference becomes zero or $T_6 = T_c = T_{LNG}$. It should carefully noted that T_7 is not equal to T_{LNG}, but

$$T_7 = T_{LNG} + \frac{\dot{m}_{LNG}C_M(T_0 - T_{LNG})}{\dot{m}C} \quad (6)$$

from Eq. (4) and

$$T_5 = T_{LNG} - \frac{\dot{m}_{LNG}i_{fg}}{\dot{m}C} \quad (7)$$

from Eq. (5). Since the RHX is balanced with 100% effectiveness, T_7 is equal to T_4, and the isentropic relation for the expander becomes

$$\frac{T_7}{T_5} = \left(\frac{P_H}{P_L}\right)^{(\gamma-1)/\gamma} \quad (8)$$

where γ is the specific ratio of gas refrigerant. By combining Eqs. (6)–(8), the required mass flow rate of refrigerant ($\dot{m}$) may be derived as a function pressure ratio (P_H/P_L)

$$\dot{m} = \dot{m}_{LNG}\frac{C_M(T_0 - T_{LNG}) + i_{fg}(P_H/P_L)^{(\gamma-1)/\gamma}}{CT_{LNG}[(P_H/P_L)^{(\gamma-1)/\gamma} - 1]} \quad (9)$$

In order to consider thermodynamic efficiency, the entropy generation rate at the LHX can be calculated as

$$(\dot{S}_{gen})_{LHX} = \dot{m}(s_7 - s_5) - \dot{m}_{LNG}[(s_a - s_c) + (s_c - s_d)] \quad (10)$$

which may be expressed in terms of pressure ratio and the properties of methane as

$$(\dot{S}_{gen})_{LHX} = \dot{m}R\ln\frac{P_H}{P_L} - \dot{m}_{LNG}\left(C_M\ln\frac{T_0}{T_{LNG}} + \frac{i_{fg}}{T_{LNG}}\right) \quad (11)$$

Since $\dot{m}$ and (P_H/P_L) are dependent each other as Eq. (9), the entropy generation rate can be expressed as a function of (P_H/P_L). No entropy is generated in RHX as the two flows are balanced and the effectiveness is 100%.

It is not possible in this limiting case to evaluate the actual size of heat exchangers, because 100% effectiveness may mean already an infinitely large heat exchange area. On the other hand, the heat exchange rate in RHX can be the first index of required size. The heat in RHX is given as

$$\dot{Q}_{RHX} = \dot{m}C(T_0 - T_7) = (\dot{m}C - \dot{m}_{LNG}C_M)(T_0 - T_{LNG}) \quad (12)$$

from Eq. (6). Since $\dot{m}$ and (P_H/P_L) are dependent each other as Eq. (9), $\dot{Q}_{RHX}$ can be expressed as a function of (P_H/P_L) only.

Fig. 3a and b are the plots for Eqs. (11) and (12), respectively. It can be observed that a smaller (P_H/P_L) is preferred for higher thermodynamic efficiency (small entropy generation), while a larger (P_H/P_L) is preferred for compactness of the recuperative heat exchanger. This conclusion is consistent with the general characteristics of Brayton refrigeration cycle between two thermal reservoirs [7], because the latent heat from Eq. (5) is dominant over the sensible heat from Eq. (4) in the refrigeration load for liquefying methane. It should be noted, however, that the same statement may not be true for the liquefaction of nitrogen or hydrogen, where the sensible heat load is dominant over the latent load.

In selecting refrigerant, it is also concluded that nitrogen is preferred for thermodynamic efficiency, while helium is preferred for compactness of recuperative heat exchanger. For the present application, nitrogen is selected, since the entropy generation may be reduced at least by 10% when the pressure ratio is around 3.

2.3. Modified reversed-Brayton cycle

Before proceeding with detailed system design, a short discussion will be given about the question whether the modification of cycle shown in Fig. 1b is favorable in thermodynamic efficiency. In order to compare this modified system with the standard system, a similar cycle analysis is presented based upon the same simplifying assumptions as the previous section.

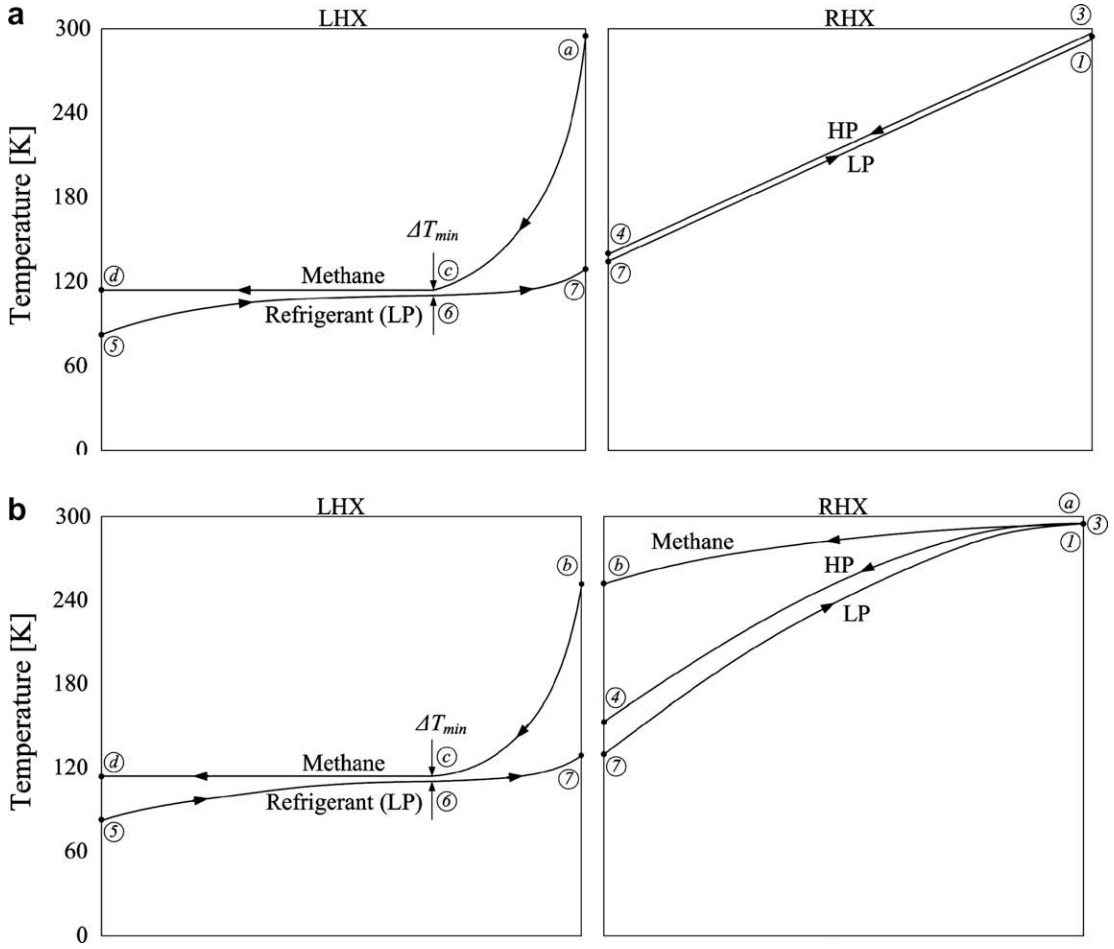

Fig. 2. Sketch of temperature distributions in liquefying heat exchanger (LHX) and recuperative heat exchanger (RHX): (a) standard cycle; (b) modified cycle.

The energy balance equations for RHX and two parts of LHX can be written as

$$\dot{m}C(T_0 - T_7) = \dot{m}C(T_0 - T_4) + \dot{m}_{LNG}C_M(T_0 - T_b) \tag{13}$$

$$\dot{m}C(T_7 - T_{LNG}) = \dot{m}_{LNG}C_M(T_b - T_{LNG}) \tag{14}$$

$$\dot{m}C(T_{LNG} - T_5) = \dot{m}_{LNG}i_{fg} \tag{15}$$

because $T_3 = T_1 = T_a = T_0$ and $T_6 = T_c = T_{LNG}$. Since the RHX is a triple-passage heat exchanger where the cold (and low-pressure) stream is in simultaneous thermal contact with the warm (and high-pressure) stream and the feed gas of methane, the ratio (r) of recuperative heat to the total heat in Eq. (12) is defined here as

$$r = \frac{\dot{m}C(T_0 - T_4)}{\dot{m}C(T_0 - T_7)} \quad \text{or} \quad 1 - r = \frac{\dot{m}_{LNG}C_M(T_0 - T_b)}{\dot{m}C(T_0 - T_7)} \tag{16}$$

In practice, the recuperative ratio can be set at an intended value with a number of different methods such as selecting a variety of heat exchanger types, installing an extended surface, or controlling flow conditions, and its effect on thermal interaction has been reported in detail earlier [8]. It is noted that the modified cycle is simply the standard cycle, if $r = 1$.

In a similar way as the previous section, the four unknown temperatures (T_4, T_5, T_7, T_b) can be determined when r and P_H/P_L are given. First, Eqs. (13) and (14) are rearranged for T_7, respectively as

$$T_7 = T_4 - \frac{\dot{m}_{LNG}C_M}{\dot{m}C}(T_0 - T_b) = T_{LNG} + \frac{\dot{m}_{LNG}C_M}{\dot{m}C}(T_b - T_{LNG}) \tag{17}$$

which can be solved for T_4 as

$$T_4 = T_{LNG} + \frac{\dot{m}_{LNG}C_M}{\dot{m}C}(T_0 - T_{LNG}) \tag{18}$$

And Eq. (15) is rearranged as

$$T_5 = T_{LNG} - \frac{\dot{m}_{LNG}i_{fg}}{\dot{m}C} \tag{19}$$

Now Eqs. (18) and (19) are substituted into the isentropic relation for the expander

$$\left(\frac{P_H}{P_L}\right)^{(\gamma-1)/\gamma} = \frac{T_4}{T_5} = \frac{T_{LNG} + \frac{\dot{m}_{LNG}C_M}{\dot{m}C}(T_0 - T_{LNG})}{T_{LNG} - \frac{\dot{m}_{LNG}i_{fg}}{\dot{m}C}} \tag{20}$$

to end up with the same expression as Eq. (9).

The entropy generation rate should be added for RHX and LHX, because there is finite ΔT in the RHX for $r < 1$ even though the effectiveness may be 100%. The sum of entropy generation in the two heat exchangers can be written as

$$(\dot{S}_{gen})_{RHX+LHX} = \dot{m}[(s_1 - s_7) + (s_4 - s_3) + (s_7 - s_5)] - \dot{m}_{LNG}[(s_a - s_c) + (s_c - s_d)] \tag{21}$$

which may be simplified as

$$(\dot{S}_{gen})_{RHX+LHX} = \dot{m}R\ln\frac{P_H}{P_L} - \dot{m}_{LNG}\left(C_M \ln\frac{T_0}{T_{LNG}} + \frac{i_{fg}}{T_{LNG}}\right) \tag{22}$$

with Eq. (8), Eqs. (13)–(16), and other thermodynamic relations. It should be noted again that the entropy generation is independent

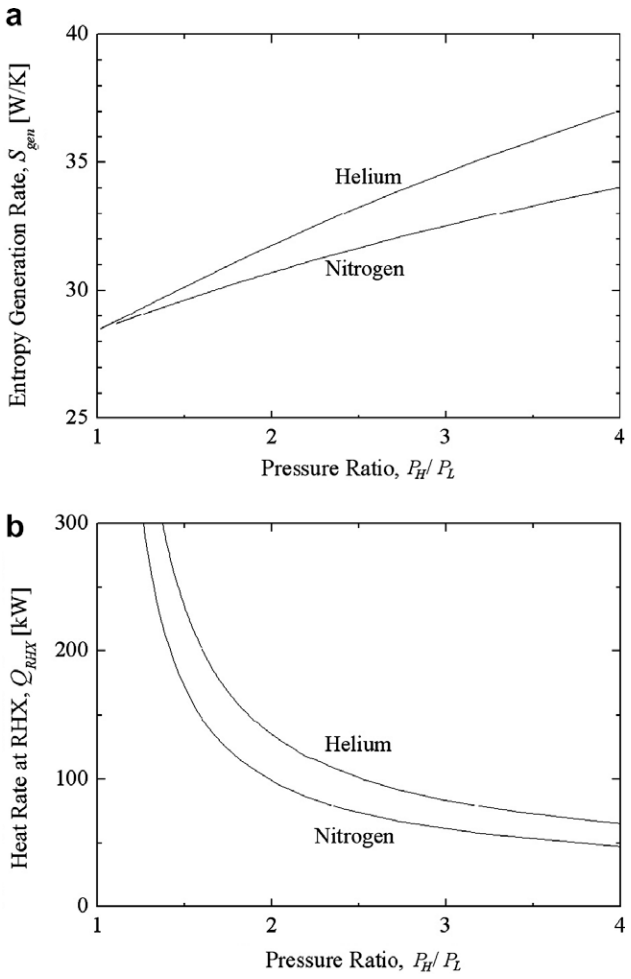

Fig. 3. Effect of pressure ratio for nitrogen and helium as refrigerant in standard cycle to produce LNG at rate of 18.5 g/s: (a) entropy generation rate at LHX; (b) heat rate at RHX.

of r, and the overall thermodynamic performance of the modified cycle is basically the same as the standard cycle.

This result has an important implication in deciding the cycle configuration. A major motivation for modifying the standard cycle is to reduce the entropy generation due to large temperature difference at the entrance region of methane gas. The reduction of entropy generation in the LHX is effective, when $r < 1$. On the other hand, the partial cooling of methane results in an imbalance of counterflow in the RHX, which is followed by a larger temperature difference at the cold end or an increase of entropy generation in the RHX. The analytical result given by Eq. (22) means that the two effects have the same impact in opposite direction. Even though this is the case of highly effective heat exchangers, it may be carefully stated that this specific modification of cycle is not obviously superior in thermodynamic efficiency to the standard cycle. In this context, the detailed design for prototype construction is devoted only to the standard reversed-Brayton cycle.

3. Heat exchanger design

Thermodynamic investigation presented above is based on 100% effective heat exchangers that can be closely realized with an enormous size. Since one of the design goals is to make the system compact, it is a practically significant issue to pursue the best performance for a given total size of heat exchangers. In order to demonstrate and discuss a detailed design procedure, a specific type of cryogenic heat exchanger is selected for both RHX and LHX, and the size issues are treated.

Among a number of options [4,9], plate-fin heat exchangers are suitable for this application, mainly because they are easily packaged onto skids and flexible in integrating different purification modules. As schematically shown in Fig. 4, the heat exchangers are constructed by stacking alternate layers of corrugated aluminum sheets (fins) between flat aluminum separator plates to for individual passages.

In RHX, the temperature distributions of low-pressure (LP) and high-pressure (HP) streams are determined by a set of energy balance equations

$$\dot{m}C_{LP}\frac{dT_{LP}}{dz} = U_{RHX}P_e(T_{HP} - T_{LP}) \tag{23}$$

$$\dot{m}C_{HP}\frac{dT_{HP}}{dz} = -U_{RHX}P_e(T_{HP} - T_{LP}) \tag{24}$$

where $U_{RHX}P_e$ is the product of overall heat transfer coefficient and effective perimeter, which can be expressed with thermal resistance model for a heat exchanger having fins on both sides. With notations shown in Fig. 4,

$$\frac{1}{U_{RHX}P_e} = \frac{1}{nW}\left[\frac{w+t}{h_{HP}(w+\eta_{HP}l)} + \frac{t}{k_{Al}} + \frac{w+t}{h_{LP}(w+\eta_{LP}l)}\right] \tag{25}$$

where the fin efficiency is given by

$$\eta = \frac{\tanh\left(\frac{l}{2}\sqrt{\frac{2h}{k_{Al}t}}\right)}{\frac{l}{2}\sqrt{\frac{2h}{k_{Al}t}}} \tag{26}$$

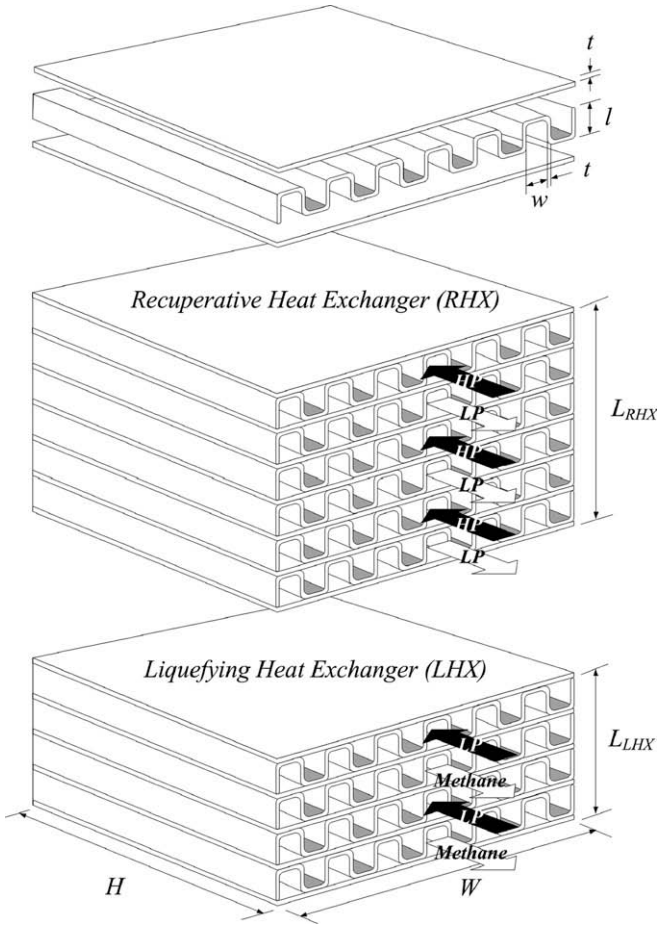

Fig. 4. Structure and dimensional notations of plate-fin heat exchanger.

because the fin is considered a plate whose thickness is t and length from the base is $l/2$ by symmetry. The convective heat transfer coefficient in Eqs. (25) and (26) is estimated with engineering correlations for fully developed flow in a channel [10]

$$h = \begin{cases} \frac{k}{d}Nu & \text{(laminar)} \\ 0.023\frac{k}{d}Re^{0.8}Pr^{1/3} & \text{(turbulent)} \end{cases} \tag{27}$$

where d is the hydraulic diameter of rectangular channel, defined as

$$d = \frac{2wl}{w+l} \tag{28}$$

For the physical dimensions listed in Table 1, the aspect ratio is 1 or $Nu \approx 3.61$ [10] for a laminar flow. In most of practical cases under consideration, every flow in the channel is turbulent.

In LHX, the heat exchanger design is more complicated, since the methane flow should be treated in different ways for the two regions. In the vapor region, the energy balance equations the temperature distributions of low-pressure (LP) and methane (M) streams are similar with RHX. In the condensation region, however, the enthalpy change in the flow direction should be expressed in terms of the quality (x_M = the mass fraction of vapor in liquid–vapor mixture). The energy balance equations are written as

$$\dot{m}C_{LP}\frac{dT_{LP}}{dz} = U_{LHX}P_e(T_M - T_{LP}) \tag{29}$$

$$\left.\begin{matrix} \dot{m}C_M\frac{dT_M}{dz} \text{ (vapor)} \\ \dot{m}\frac{dx_M}{dz}i_{fg} \text{ (condensation)} \end{matrix}\right\} = -U_{LHX}P_e(T_M - T_{LP}) \tag{30}$$

where $U_{LHX}P_e$ may be estimated similarly as Eqs. (25)–(28). In the condensation region, the condensing heat transfer coefficient may be approximated by

$$h = 0.555\left[\frac{\rho g(\rho-\rho_v)k^3 i_{fg}}{\mu(T_{LNG}-T_s)d}\right]^{1/4} \tag{31}$$

This empirical correlation is valid for vapor condensation with low velocity in a horizontal tube [10], but any more precise estimation is not necessary, because the heat transfer coefficient for condensation is much greater than the low-pressure stream and does not affect the overall heat transfer.

The heat exchanger performance is rigorously calculated by solving numerically the differential equations with incorporating the commercial code developed by the US NIST [11] for thermophysical properties of methane and nitrogen. Fourth-order Runge–Kutta method is employed for numerical integration and so-called "shooting method" is employed to impose the boundary conditions. In order to investigate the effect of heat exchanger size, it is assumed in this design that a pair of unit exchanger is fixed at a plate area of $W \times H$ and corrugated fins with (w,l,t) but the number of stacks (or L) is a variable.

4. Cycle analysis

Cycle analysis program is shortly completed, if the heat exchanger modules for LHX and RHX are linked. Since the aftercooler is located outside the cold box and state 3 can be easily cooled to room temperature, it is assumed here that $T_3 = T_0$. It is also assumed that adiabatic efficiency is given a number for compressor and expander, which is defined as

$$\eta_c = \frac{i(P_H, s_1) - i_1}{i_2 - i_1} \tag{32}$$

$$\eta_e = \frac{i_4 - i_5}{i_4 - i(P_L, s_4)} \tag{33}$$

respectively. The efficiency is in the range of 70–85% for contemporary compressors or expanders available to this application. The results in the following sections are obtained on 85% for aiming at the best performance design. The required mass flow rate of refrigerant is determined with the energy balance at LHX

$$\dot{m} = \dot{m}_{LNG}\frac{i_a - i_d}{i_7 - i_5} \tag{34}$$

When P_H, P_L, L_{RHX} and L_{LHX} are given, every state in the cycle can be uniquely determined. Thermodynamic properties of methane and refrigerant are accurately calculated with commercial program [11].

Net power is the difference between the power input at compressor and the power output at expander

$$\dot{W} = \dot{m}[(i_2 - i_1) - (i_4 - i_5)] \tag{35}$$

Eqs. (1), (34), and (35) are substituted into Eq. (2), yielding FOM in terms of enthalpy at several states of the cycle

$$\text{FOM} = \frac{i_7 - i_5}{(i_2 - i_1) - (i_4 - i_5)}\left[\frac{T_0(s_0 - s_{LNG})}{(i_0 - i_{LNG})} - 1\right] \tag{36}$$

Table 1
Specifications of plate-fin heat exchanger

Material	Aluminum
Heat exchanger width, W	1 m
Heat exchanger height, H	1 m
Total heat exchanger length, L	1 m
RHX length, L_{RHX}	0.6 m
LHX length, L_{LHX}	0.4 m
Flow channel height, l	23 mm
Flow channel width, w	23 mm
Plate thickness, t	1 mm

5. Results and discussion

5.1. Operating pressure

The most important design parameter in the liquefaction system is the operating pressure. As demonstrated in Fig. 3, the pressure ratio should be smaller for a better thermodynamic efficiency in standard reversed-Brayton cycle, mainly because the entropy generation due to temperature difference in LHX is smaller. This is true, however, only if the heat exchanger effectiveness is 100% or the size of RHX and LHX is infinitely large. Since compactness is one of the design goals, it is practically significant to study the effect of pressure ratio for a fixed size of heat exchangers as constraint.

Fig. 5 and 6 are the required mass flow rate and the estimated FOM as a function of pressure ratio, when $L_{RHX} = 0.6$ m and $L_{LHX} = 0.4$ m. Nitrogen is the refrigerant, and the adiabatic efficiency of the compressor and expander is 0.85, respectively, assuming high performance machines in practice. Other conditions in the cycle analysis are listed in Table 1. In Fig. 5, the practical cycle is compared with a reference to the standard cycle, where the heat exchanger effectiveness is 100% for both RHX and LHX. As the pressure ratio increases, the required mass flow decreases monotonically, but FOM increases up to 0.26 then gradually decreases. The optimal pressure ratio to maximize the thermodynamic efficiency turns out to be approximately 3 in the specific conditions. As a lower pressure ratio, the required mass flow of refrigerant is exceedingly larger, which result in a poor heat exchange performance with the given size.

This optimal value of pressure ratio might not be applicable to every reversed-Brayton cycle in general. It is obvious in comparison with the standard cycle that the optimal pressure ratio should be smaller, if the given size of heat exchangers is greater. However, the pressure ratio may well be selected at around 3 for the prototype design of methane liquefaction system.

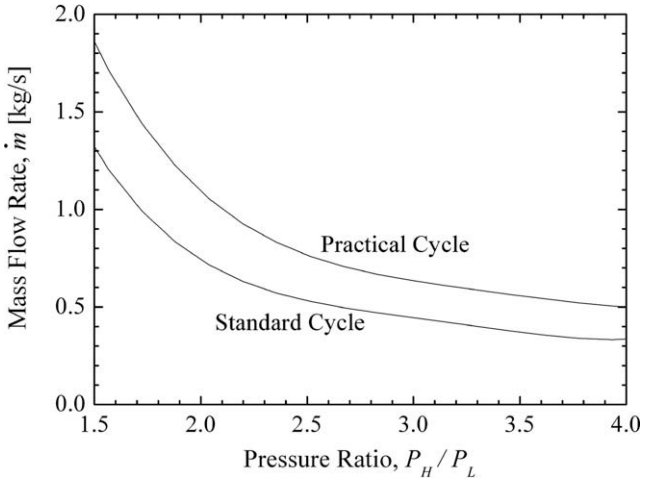

Fig. 5. Required mass flow rate of refrigerant as a function of pressure ratio for standard cycle and practical cycle (L_{RHX} = 0.6 m, L_{LHX} = 0.4 m).

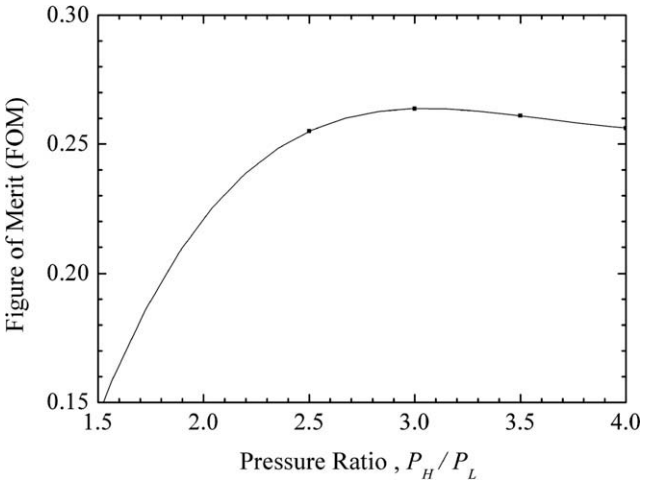

Fig. 6. Figure of merit as a function of pressure ratio (L_{RHX} = 0.6 m, L_{LHX} = 0.4 m).

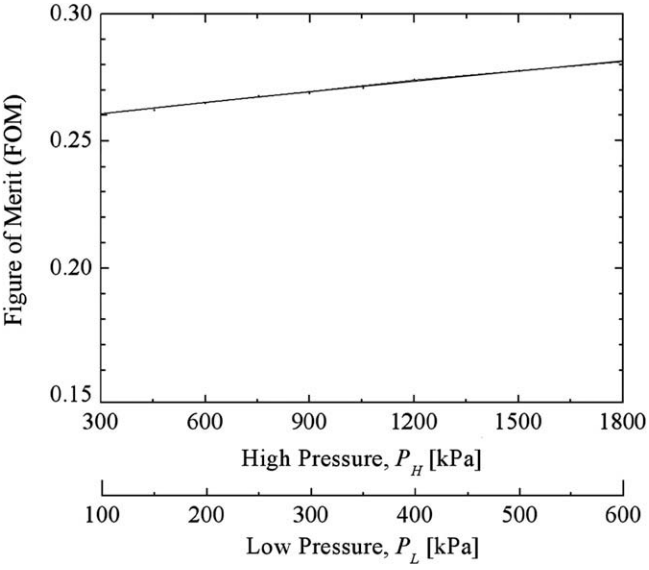

Fig. 7. Figure of merit as a function of operating pressure (P_H/P_L = 3).

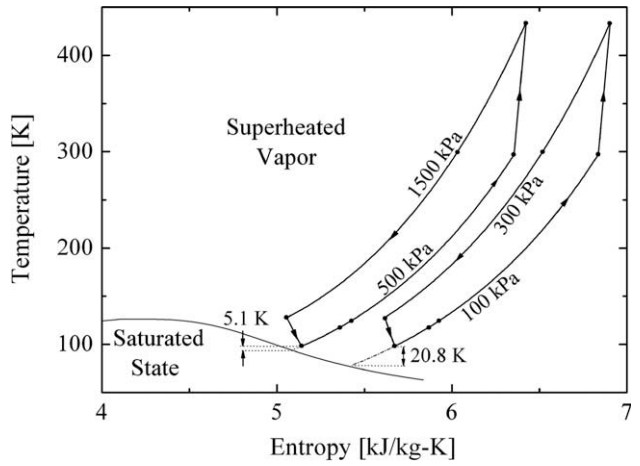

Fig. 8. Two cycles on temperature–entropy diagram, which has same pressure ratio (P_H/P_L = 3) but different pressure range.

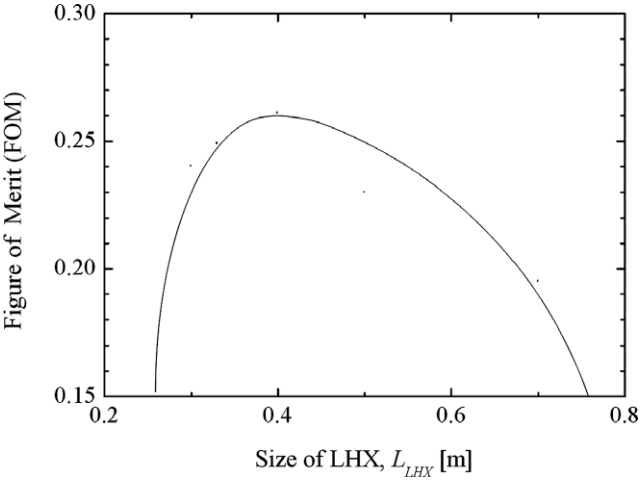

Fig. 9. Figure of merit as a function of size of liquefying heat exchanger (LHX) when the total heat exchanger size is fixed as $L_{LHX} + L_{RHX}$ = 1 m.

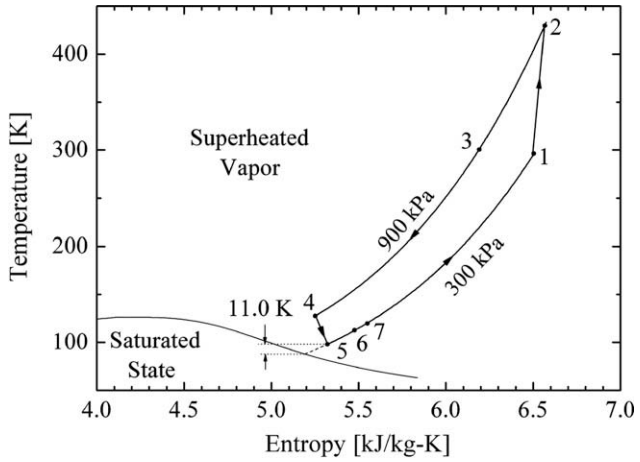

Fig. 10. Reversed-Brayton cycles for prototype on temperature–entropy diagram.

Another issue is how to choose the combination of high and low pressures that yields the optimal pressure ratio. As demonstrated earlier, the thermodynamic performance of standard cycle is

Table 2
Summary of designed cycle with properties at each state

	Nitrogen, $\dot{m} = 650$ g/s					Methane, $\dot{m}_{LNG} = 18.5$ g/s			
	P (kPa)	T (K)	i (kJ/kg)	s (kJ/kg K)		P (kPa)	T (K)	i (kJ/kg)	s (kJ/kg K)
1	300	297.3	307.9	6.508	a	101.3	298.0	621.5	11.60
2	900	434.1	450.3	6.567	c	101.3	111.7	223.4	9.508
3	900	298.0	307.3	6.180	d	101.3	111.7	−278.4	5.013
4	900	127.8	122.2	5.252					
5	300	98.1	96.16	5.321	$\dot{W}_{min} = 19.9$ kW				
6	300	110.9	110.7	5.461	$\dot{W} = \dot{W}_{COMP} - \dot{W}_{EXP} = 92.6 - 16.9 = 75.7$ kW				
7	300	122.5	123.5	5.570	FOM = 0.263				

dependent only the ratio, not the two values of pressure. In practical cycle, the operating pressure affects the fluid properties and the effectiveness of heat exchangers. The cycle analysis is repeated for different pressure combinations whose ratio is 3, and the results are plotted in Fig. 7. Even though the effect of pressure may be meager, a slightly higher FOM may be obtained with an elevated pressure. On the other hand, as the pressure range increases, the state 4 (exit of expander) gets closer to the saturation region of nitrogen as demonstrated by two cases in Fig. 8. The proximity to saturation means a possibility of liquid nitrogen in the expander, which may seriously shorten the life of expensive cryogenic rotor by erosion. In this specific case, the exit state enters the saturated region at a pressure range higher than the combination of 2100–700 kPa. With a safety margin of 10 K in preparation for off-design operation, the operating pressure in present design is selected as 900–300 kPa.

5.2. Size of heat exchangers

The thermodynamic efficiency can be improved if the size of LHX or RHX is increased. Since the impact of size may be different for the two heat exchangers, it is a practically crucial design issue to determine their relative size when the total size is given as constraint. Fig. 9 is a plot of FOM as a function of L_{LHX}, when $L_{LHX} + L_{RHX} = 1$ m. In the calculation, the operating pressure is selected optimally as $P_H = 900$ kPa and $P_L = 300$ kPa. There exists a clear optimal L_{LHX} at around 0.35–0.40 m for thermodynamic efficiency to have the maximum. In present design, the best relative size of LHX and RHX is suggested to be 40% and 60%, respectively. It is noted that the shape of curve in Fig. 9 is sharply peaked near the top and drops sharply as the size of LHX gets away from the optimum. This implies the practical importance of present design issue in pursuing thermodynamic efficiency and compactness at the same time.

It is noticeable that the optimal ratio of 40:60 is far greater than the ratio of heat exchange rates for RHX and LHX, which is nearly 1:7 in this system. The main reason is that the entropy generation due to temperature difference in a heat exchanger is more crucial at lower temperatures. A well-known optimization principle for cryogenic heat exchangers [7]

$$\left(\frac{\Delta T}{T}\right)_{opt} = \text{constant} \tag{37}$$

may be reminded here.

5.3. Summary of prototype design

To reach the immediate objective of this study, detailed specifications are developed for a prototype of methane liquefaction system. The specifications of the two exchanger design are listed in Table 1 in case that $L_{RHX} + L_{LHX} = 1$ m is optimally divided at 60:40. The operating pressure is determined in consideration of thermodynamic efficiency and a design constraint on the degree of superheating to avoid the condensation of nitrogen. The finally suggested thermodynamic cycle is plotted on T–s diagram of nitrogen as Fig. 10, and the corresponding properties at each state are listed in Table 2. The net input power is estimated at 75.7 kW or the FOM of the liquefaction system is estimated at 26.3%. The two heat exchangers may be compactly packed in 1 m × 1 m × 1 m or a slightly larger volume.

6. Conclusions

A rigorous thermodynamic study is performed to develop detailed specifications of methane liquefaction system based on reversed-Brayton cycle, which may be directly applicable to LFG-to-LNG conversion technology in a distributed scale. The real properties of refrigerant, the heat transfer coefficients, and the heat exchanger performance with phase change process are taken into full consideration. Some significant and specific conclusions are obtained through the results of system design as followings.

Nitrogen is a superior refrigerant to helium, since required power may be saved at least by 10%. On the other hand, care should be taken in the cycle design to avoid liquid nitrogen in expander. The modification of reversed-Brayton cycle that the feed gas is precooled through recuperative heat exchanger (RHX) is not notably helpful in improving thermodynamic efficiency or compactness of the system. It is verified that for a fixed size of heat exchangers, there exists an optimum for the pressure ratio to maximize the thermodynamic efficiency, and the optimal pressure ratio is suggested as 3 in the prototype to be constructed. When sum of the two heat exchanger sizes is given by constraint, the distribution ratio of 40:60 for LHX and RHX is recommended for the best thermodynamic performance.

The presented results will be directly applied to a liquefaction module in the prototype of LNG production system. As mentioned, a minor modification may be followed while integrating with the separation and purification modules to treat the LFG. According to the proposed schedule, the construction of prototype will be completed by the middle of 2009 on a waste landfill site at Metropolitan Seoul.

Acknowledgments

This research has been supported by the development project, "LNG Production and CO_2 Recovery Technology through Liquefaction Process of Biogas," funded by the Korea New and Renewable Energy Center (KNREC).

References

[1] Gongaware DF, Barclay MA, Barclay JA, Skrzypkowski MP. Conversion of waste gas to liquid natural gas. Adv Cryog Eng 2004;49:83–90.
[2] Fan QH, Li HY, Yin QS, Jia LX. In: 2007 Cryogenic engineering conference and international cryogenic materials conference, July 2007. Paper # C3-D-03.
[3] Barclay MA, Gongaware DF, Dalton K, Skrzypkowski MP. Thermodynamic cycle selection for distributed natural gas liquefaction. Adv Cryog Eng 2004;49:75–82.

[4] Timmerhaus KD, Flynn TM. Cryogenic process engineering. New York and London: Plenum Press; 1989.
[5] Andress DL, Watkins RJ. Beauty of simplicity: Phillips optimized cascade LNG liquefaction process. Adv Cryog Eng 2004;49:91–8.
[6] Website of Stirling Cryogenics & Refrigeration BV. <www.stirling.nl>.
[7] Bejan A. Advanced engineering thermodynamics. 3rd ed. New Jersey: John Wiley & Sons; 2006.
[8] Cho YH, Chang HM. An effectiveness-NTU method for triple-passage counterflow heat exchangers. KSME J 1993;7(3):232–89.
[9] Kays WM, London AL. Compact heat exchangers. 3rd ed. New York: McGraw-Hill; 1984.
[10] Incropera FP, Dewitt DP. Introduction to heat transfer. 4th ed. New York: John Wiley & Sons; 2001.
[11] Friend DG. NIST Thermophysical properties of pure fluids. Version 3.0. Boulder: NIST; 1992.